

HIV-1 IN Strand Transfer Chelating Inhibitors: A Focus on Metal Binding

Alessia Bacchi,[†] Mauro Carcelli,[†] Carlotta Compari,[‡] Emilia Fiscaro,[‡] Nicolino Pala,[§] Gabriele Rispoli,[†] Dominga Rogolino,^{*,†} Tino W. Sanchez,^{||} Mario Sechi,[§] and Nouri Neamati^{||}

[†]Dipartimento di Chimica Generale ed Inorganica, Chimica Analitica, Chimica Fisica and [‡]Dipartimento di Scienze Farmacologiche, Biologiche e Chimiche Applicate, Università di Parma, Parco Area delle Scienze, 17/A, 43124 Parma, Italy

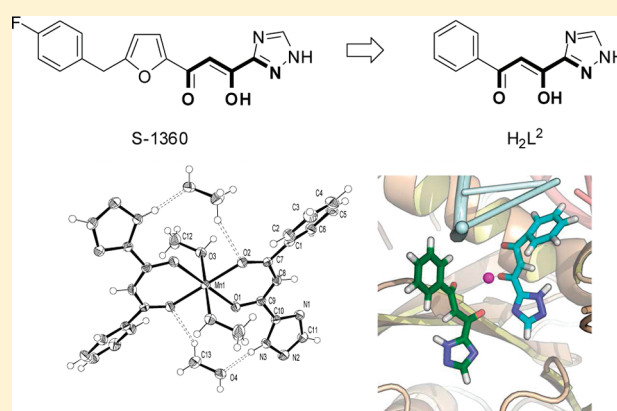
[§]Dipartimento Farmaco Chimico Tossicologico, Università di Sassari, Via Muroni 23/A, 07100 Sassari, Italy

^{||}Department of Pharmaceutical Sciences, School of Pharmacy, University of Southern California, 1985 Zonal Avenue, PSC 304, Los Angeles, California 90089, United States

S Supporting Information

ABSTRACT: Most active and selective strand transfer HIV-1 integrase (IN) inhibitors contain chelating functional groups that are crucial feature for the inhibition of the catalytic activities of the enzyme. In particular, diketo acids and their derivatives can coordinate one or two metal ions within the catalytic core of the enzyme. The present work is intended as a contribution to elucidate the mechanism of action of the HIV-IN inhibitors by studying the coordinative features of H_2L^1 (L-708,906), an important member of the diketo acids family of inhibitors, and H_2L^2 , a model for S-1360, another potent IN inhibitor. Magnesium(II) and manganese(II) complexes of H_2L^1 and H_2L^2 were isolated and fully characterized in solution and in the solid state. The crystal structures of the manganese complex $[Mn(HL^2)_2(CH_3OH)_2] \cdot 2CH_3OH$ were solved by X-ray diffraction analysis. Moreover, the speciation models for H_2L^2 with magnesium(II) and manganese(II) ions were performed and the formation constants of the complexes were measured. $M(HL^2)_2$ ($M = Mg^{2+}, Mn^{2+}$) was the most abundant species in solution at physiological pH. All the synthesized compounds were tested for their anti-IN activity, showing good results both for the ligand and the corresponding complexes. From analysis of the speciation models and of the biological data we can conclude that coordination of both metal cofactors could not be strictly necessary and that inhibitors can act as complexes and not only as free ligands.

KEYWORDS: HIV-1 integrase, strand transfer selective inhibitors, S-1360, metal complexes, coordinating pharmacophores



INTRODUCTION

The antiviral therapy currently in use against the human immunodeficiency virus type 1 (HIV-1) provides good results, coming close to stopping viral evolution. However, it does not completely suppress viral replication in cells, and several factors like drug toxicity, resistant strains and problems with patient adherence clearly indicate the necessity to develop new and more potent drugs. In the last ten years, HIV-1 integrase (IN), which catalyzes the integration of proviral cDNA into the host cell genome,^{1–7} has emerged as a promising target for drug design. The efforts in this direction resulted in the recent approval by the US FDA of the first IN inhibitor, raltegravir (brand name Isentress, Merck & Co.).⁸ Currently, there are several other IN inhibitors under clinical trial (Figure 1).⁹

IN is a 32 kDa protein that folds into three domains: the C-terminal domain, the N-terminal domain and the catalytic core domain. The core domain contains the “D,D(35)E” motif that is

highly conserved among polynucleotidyl transferases.¹⁰ These three conserved amino acid residues coordinate one or two divalent metal ions. IN catalyzes the insertion of the viral DNA into the host cell genome through two different steps, 3'-processing and strand transfer. During 3'-processing IN selectively cleaves the last two nucleotides (GT) of viral DNA, to generate two CA-3'-hydroxyl recessed ends, which are the reactive intermediates required for the next step. The enzyme, still bound to the 3'-processed viral DNA, translocates to the nucleus of the infected cell as a part of the preintegration complex, wherein the terminal 3'-OH of the viral DNA attacks the host DNA in the strand transfer step.

Received: October 8, 2010

Accepted: February 16, 2011

Revised: February 9, 2011

Published: February 16, 2011

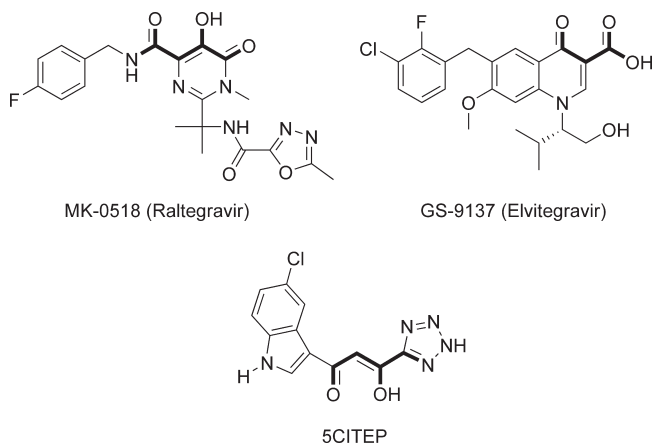


Figure 1. HIV-1 IN inhibitors raltegravir, elvitegravir and 5CITEP.

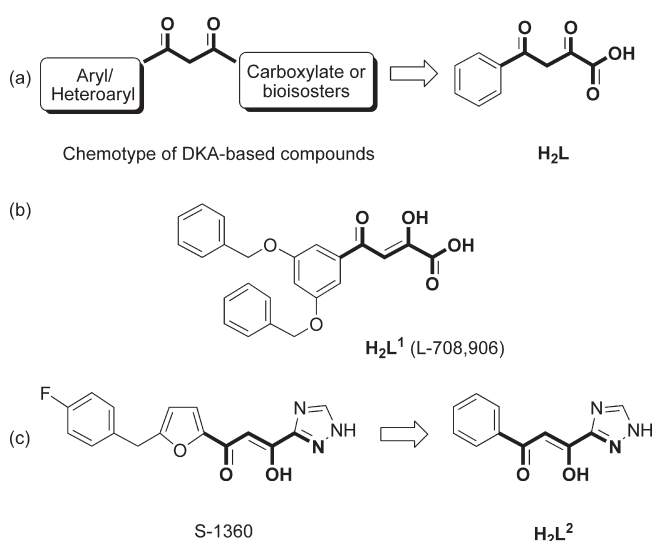


Figure 2. (a) Chemotype of DKA β -diketo-based inhibitors; (b) H₂L¹; (c) the triazolic bioisostere S-1360 with its model H₂L² used in the present work.

Several classes of IN inhibitors have been identified, dating back to the studies on diketo acids (DKAs, Figure 2a) and their bioisosteres, such as the keto-enol tetrazole 5CITEP (Figure 1) and the keto-enol triazole S-1360 (Figure 2c),^{11–14} until the more recent examples, carboxamide^{15–17} and quinolone derivatives.^{18–21} The keto-enolic acid motif can be replaced by several bioisosteres that can mimic a ketone, an enol and a carboxyl moiety. The presence of this common scaffold is thought to be fundamental for inhibition, since it allows the coordination of the divalent metal ions, i.e. the possibility to block the active site by competing with the viral DNA substrate (Figure 3). These considerations have been recently supported by the resolution of the X-ray structure of the full-length enzyme in complex with the viral DNA, in the absence and in the presence of inhibitors.²² The crystal structure of the intasome (the complex between viral DNA and IN) with raltegravir and elvitegravir shows that they are located within the active site with their chelating fragments oriented toward the metal cofactors, while the benzyl groups fit within a tight pocket of the enzyme. Several studies^{23–26} have pointed out the critical importance of the hydrophobic substituent adjacent to the pharmacophoric

chelating groups. Modification of the hydrophobic scaffold can in fact produce a dramatic variation of activity. This is probably due to the fact that this moiety provides a series of interactions within the active site, as precisely observed in the solved crystal structure of the intasome.²²

It is worth noting that magnesium is the metal cofactor in many processes involving formation and modification of phosphate chains that are fundamental for the action of polymerases, exonucleases, ribonucleases, transposases and integrases. Effectively, metal-chelating compounds have been developed as antiviral agents, and most of them have been derived exactly from DKAs.²⁷ It is therefore of great interest to gain insight into their mechanism of action, in order to design more effective drugs not only against HIV IN but also against many other viral enzymes, such as Hepatitis C Virus polymerase and Influenza endonuclease. Moreover, some DKA IN inhibitors have shown anti-RNase H activity,^{28–30} and recently some inhibitors of both enzymes have been identified.^{30,31}

The “two-metal ions binding model” has been suspected for a long time and it became an important strategy for the development of new and potent IN inhibitors.^{23,32–35} As mentioned earlier, DKAs are able to coordinate one or two metal ions (in particular Mg²⁺ or Mn²⁺), since they present two binding sites: the keto-enol and the carboxylate functions. Complexes with a 2:2 ligand:metal stoichiometry were predicted by quantum chemistry calculations³⁶ and isolated in our previous studies.^{37,38} Also the investigation of the coordinative ability of members of the polyhydroxylated styrylquinoline series by X-ray crystallographic analysis³⁹ evidenced the formation of bimetallic complexes of Mg²⁺ and Cu²⁺, with a Mg–Mg distance of 3.221(1) Å, that is notably in agreement with the metal–metal distance of 3.9 Å encountered in the crystal structure of *Escherichia coli* DNA polymerase as well as of IN–DNA intasome (ranging from 3.32 to 4.46 Å). The chelating ability of ligands containing the quinolone pharmacophoric fragment was elucidated by crystallographic studies on magnesium(II) complexes^{40,41} and by a series of other studies using several computational tools.^{42,43} Nevertheless, the data regarding the metal/inhibitors equilibria or regarding the biological activity of isolated metal complexes are surprisingly scarce. Moreover, it is not definitively stated if it is strictly necessary for the ligand to coordinate both metal ions or it is sufficient to block only one cation to inhibit strand transfer. In fact, the recent development of novel quinolone HIV-1 IN strand-transfer inhibitors^{18,19,44} (for example elvitegravir,⁴⁵ Figure 1, that is currently undergoing phase III clinical trials) pointed out that a monoketo acid fragment can be an alternative to the keto-enol acid motif. Therefore, an in-depth understanding of their coordinating ability is of paramount importance, since it will allow a more efficient drug design of potent inhibitors.

In this study we report the synthesis and characterization of two ligands, the (2Z)-2-hydroxy-4-oxo-4-(3,5-benzyloxy)phenylbut-2-enoic acid (H₂L¹, L-708,906, Figure 2b),¹¹ which exemplifies the DKA family of inhibitors, and the (Z)-3-hydroxy-1-phenyl-3-(1H-1,2,4-triazol-3-yl)prop-2-en-1-one (H₂L²), designed as a model of S-1360 (Figure 2c).⁴⁶ Since the primary aim of this study is to investigate the coordinating ability of IN strand transfer inhibitors, we used a simplified model of S-1360 to avoid long synthetic procedures, yet maintaining the pharmacophoric chelating scaffold. The magnesium(II) and manganese(II) metal complexes were synthesized and characterized, together with the X-ray crystal structure of ligand H₂L² and of [Mn(HL²)₂(CH₃OH)₂]·2CH₃OH. A series of

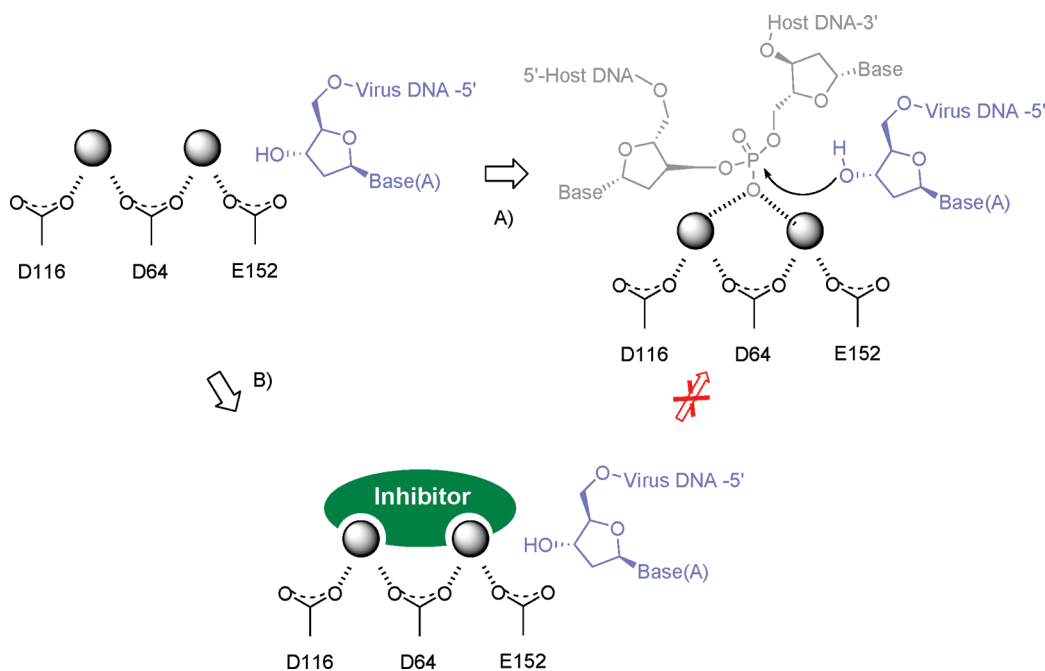
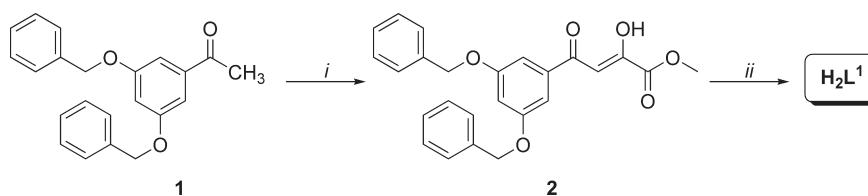


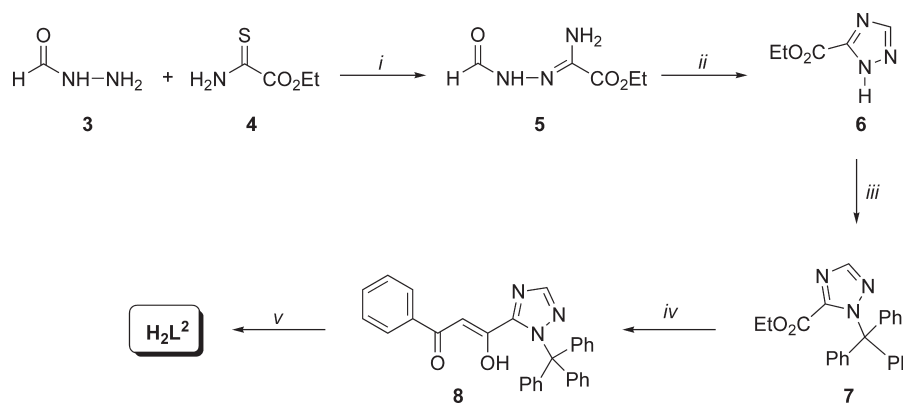
Figure 3. The two-metal inhibition mechanism. (A) Strand transfer reaction and (B) the inhibitor chelates the two metal ions blocking the host DNA binding.

Scheme 1. Preparation of Ligand H_2L^1 ^a



^a Reagents and conditions: (i) Dimethyloxalate, anhydrous DMF, NaH, 0–5 °C, then 65–70 °C for 5 h; (ii) 2 N NaOH, methanol, room temperature for 5 h, then 1 N HCl.

Scheme 2. Preparation of Ligand H_2L^2 ^a

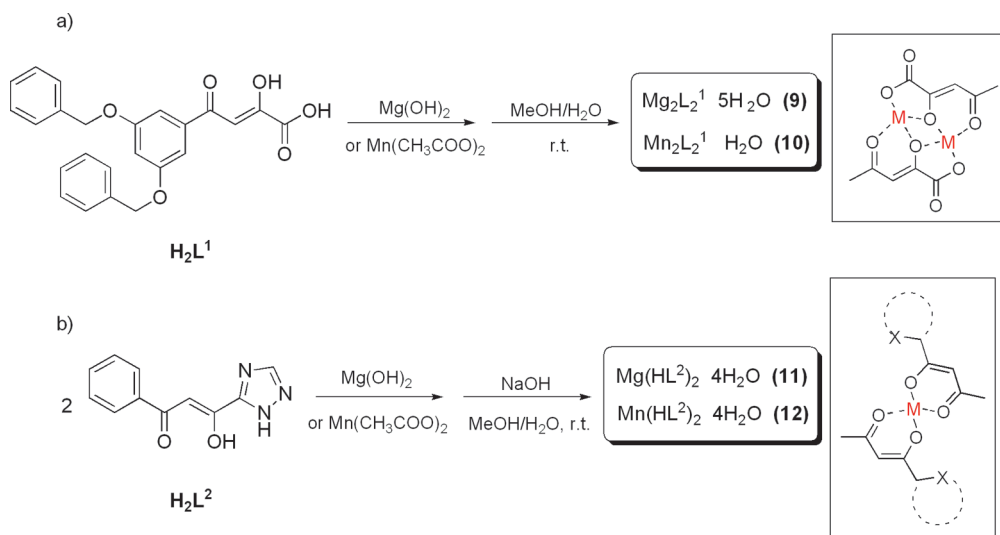


^a Reagents and conditions: (i) 65 °C, 1 h; (ii) diglyme, reflux, 1.5 h; (iii) chlorotriphenylmethane, triethylamine, anhydrous *N,N*-dimethylacetamide, rt, 15 min; (iv) acetophenone, 1 M LiHMDS in THF, anhydrous THF, –70 °C to rt, 1.5 h; (v) 3 N HCl, dioxane, 80 °C, 30 min.

potentiometric measurements were also carried out with H_2L^2 . Finally, the anti-HIV-1 IN activity of the free ligands and the related metal complexes have been evaluated in enzymatic assays, and a mechanistic hypothesis has been detailed.

RESULTS AND DISCUSSION

Chemistry. Ligand H_2L^1 (Scheme 1) was synthesized by using a modified literature procedure.^{25,47} Singlets for CH_2 protons were present at 4.58–4.60 ppm in the spectra recorded in

Scheme 3. Synthesis of Complexes 9 and 10 with Ligand H_2L^1 (a) and 11 and 12 with Ligand H_2L^2 (b)

DMSO- d_6 , indicating the coexistence of both the enolic and ketonic tautomers (98:2 and 97:3, for H_2L^1 and **2**, respectively). Moreover, a mixture of the two geometric *Z* and *E* stereoisomers was detected in a 6:1 ratio (for *E* and *Z*, respectively).⁴⁷

The ligand H_2L^2 was prepared by following the same synthetic approach we previously used for S-1360⁴⁸ (Scheme 2). It was characterized by means of IR, 1H NMR and mass spectrometry. In the 1H NMR spectrum, recorded in DMSO- d_6 , both the keto and the enolic forms are visible: the C–H proton is at 7.28 ppm (enolic form), while a singlet for the CH_2 protons of the keto tautomer is at 4.80 ppm (17%). Finally, H_2L^2 was crystallized from a MeOH/HCl solution as $H_2L^2 \cdot 1/2HCl$ and characterized by X-ray diffraction analysis (see Supporting Information).

Scheme 3a details the synthesis of complexes **9** and **10**. The ligand is bideprotonated, giving rise to dimeric complexes of type $M_2L^1_2 \cdot nH_2O$. $Mn(CH_3COO)_2$ was sufficient to deprotonate H_2L^1 , while in the case of magnesium, the hydroxide had to be used. The necessity to carefully choose the proper salt has emerged also during the studies on hydroxyisoquinoline dione dual inhibitors³⁰ so that deprotonation and therefore complexation could occur only with a sufficiently basic anion. The complete deprotonation of the ligand and the coordination of the diketo acid moiety to the metal can be inferred through the IR spectra of the complexes: the OH absorption disappeared ($2850\text{--}3100\text{ cm}^{-1}$ in the free ligand), and the $C=O$ bands shifted from 1709 (ligand) to 1679 and 1575 cm^{-1} for **9** and **10**, respectively. For complex **9**, a sharp intense band at 3695 cm^{-1} was attributable to the presence of coordinated water molecules, since it disappeared after heating the compound at $120\text{ }^\circ\text{C}$. The 1H NMR spectra of **9** confirmed the absence of acidic protons. We observed a 0.15–0.20 ppm downfield shift of all the signals vs the free ligand. Elemental analysis confirmed the proposed 1:1 stoichiometry. The DKA ligands can coordinate in the hydroxy-carboxylate⁴⁹ or in the acetyl-acetonate form.⁵⁰ In the IR spectra of **9** and **10**, the band for a free $C=O$ was absent, which allowed exclusion of the possibility that the ligand is in the hydroxy-carboxylate form. Our³⁷ and others³⁶ previous studies suggest the presence of M_2L_2 species, where both the binding modes of the ligand are

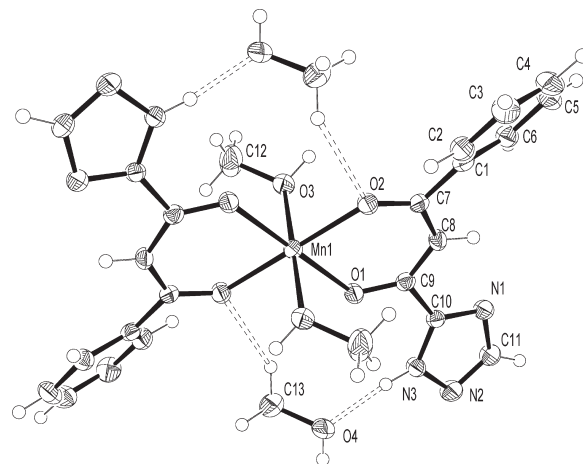


Figure 4. Crystal structure of $[Mn(HL^2)_2(CH_3OH)_2] \cdot 2CH_3OH$. Mn occupies a center of symmetry, the labeling is reported only for the independent unit. Hydrogen bonds to the pair of uncoordinated methanol molecules are dotted. Thermal ellipsoids are at the 50% probability level.

used to give a dimer where the acetyl, the hydroxy and the carboxylate groups coordinate to the metal; it can be assumed that, also for **9** and **10**, dimeric species are formed (Scheme 3a, inset).

The reactivity of H_2L^2 was slightly different. Complexes of general formula $M(HL^2)_2 \cdot 4H_2O$ ($M = Mg^{2+}$ **11**, $M = Mn^{2+}$ **12**), can be obtained by using the chloride or the acetate of the metal in the presence of a base to ensure deprotonation of the ligand (pH = 8, Scheme 3b). In these conditions, only the enolic proton is lost, while the triazolic moiety is still protonated. Monodeprotonation of the ligand and coordination were inferred by spectroscopic tools (IR, 1H NMR) and mass spectrometry and were further confirmed by X-ray diffraction analysis on the manganese complex.

Under harsh conditions (pH = 10), also the triazole ring of H_2L^2 was deprotonated, with formation of $Mg_2L^2_2 \cdot 5H_2O$ (**13**) in analogy with the DKA parent compound.³⁷ Therefore, a

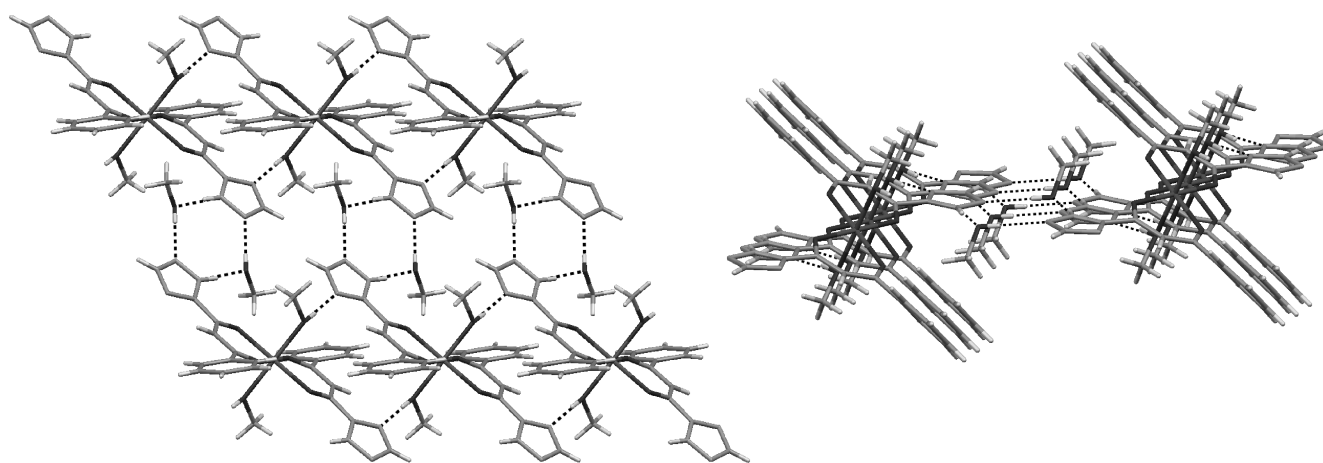


Figure 5. Frontal (left) and side-on (right) views of the supramolecular ribbons generated by hydrogen bonds (dotted) in the crystal structure of $[\text{Mn}(\text{HL}^2)_2(\text{CH}_3\text{OH})_2] \cdot 2\text{CH}_3\text{OH}$.

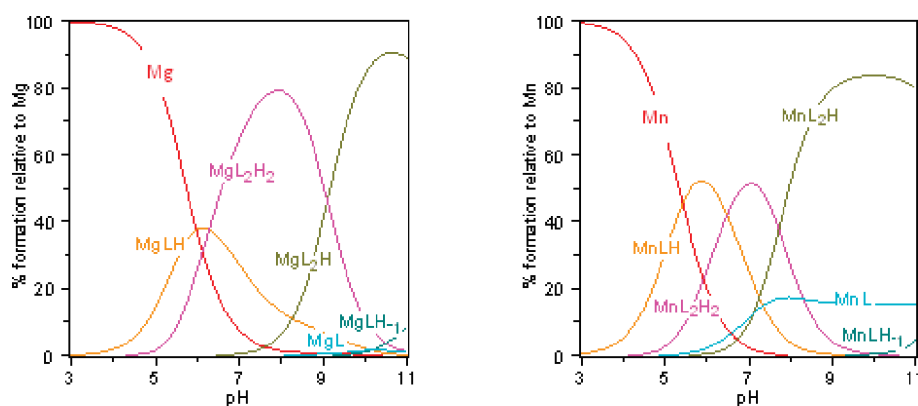


Figure 6. Distribution diagrams for the systems under investigation (ligand:M = 2:1, $[\text{H}_2\text{L}^2] = 2 \text{ mM}$).

Table 1. Logarithms of Formation Constants ($\beta_{pqr} = [\text{M}_p\text{L}_q\text{H}_r]/[\text{M}]^p[\text{L}]^q[\text{H}]^r$) in Methanol/Water = 9:1 v/v, $I = 0.1 \text{ M KCl}$ at 25°C for the Ligand under Study with Mn(II) and Mg(II)^a

<i>p</i>	<i>q</i>	<i>r</i>	M = Mn(II)	M = Mg(II)
1	1	1	16.88 (0.11)	16.60 (0.14)
1	2	1	25.32 (0.09)	23.92 (0.08)
1	2	2	33.04 (0.16)	33.02 (0.10)
1	1	-1	-2.01 (0.09)	-3.67 (0.07)
1	1	0	9.53 (0.08)	6.45 (0.32)

<i>p</i>	<i>q</i>	<i>r</i>		
0	1	1	$\text{L} + \text{H} \rightleftharpoons \text{LH}$	11.431 (0.007)
0	1	2	$\text{L} + 2\text{H} \rightleftharpoons \text{LH}_2$	19.657 (0.008)

^a Standard deviations are given in parentheses. Charges are omitted for simplicity.

coordination compound of the type $\text{M}(\text{HL}^2)_2$, with the ligand monodeprotonated, was the most abundant species at physiological conditions, but at higher pH the ligand is completely deprotonated and dimeric Mg_2L^2_2 species was also formed (see potentiometric data below).

It is interesting to note that these data are in agreement with induced-fit docking studies performed on H_2L^1 and S-1360.⁵¹

Table 2. Inhibition of HIV-1 IN Catalytic Activities of Ligands and Complexes^a

comps	<i>M</i> ^b	M:L ^c	IC ₅₀ (μM)		SI ^d
			3'-processing	strand transfer	
H_2L^1			9 ± 2	0.5 ± 0.3	18
9	Mg^{2+}	2:2	70 ± 4	1.6 ± 0.4	44
10	Mn^{2+}	2:2	4 ± 1	0.3 ± 0.1	13
H_2L^e			>333	69 ± 0.4	>5
H_2L^2			>100	43 ± 7	>2
11	Mg^{2+}	1:2	100	42 ± 16	2.4
12	Mn^{2+}	1:2	87 ± 7	19 ± 4	5
S-1360 ^f			11 ± 2	0.6 ± 1	18

^a MnCl_2 was used in the reaction buffer. ^b *M*, metal ion. ^c M:L, metal:ligand ratio. ^d SI: selectivity index. ^e Data from ref 37. ^f Data from ref 54.

While for H_2L^1 a classical two-metal chelation model has been found, two preferred binding modes have been disclosed for the triazolic bioisostere. Both models can be regarded as two-metal binding, but in one case the Mg^{2+} ions show close interactions only with the keto-enolic fragment. Other recent computational studies seem to suggest a two-metal binding also for the diketo triazole pharmacophore.⁵²

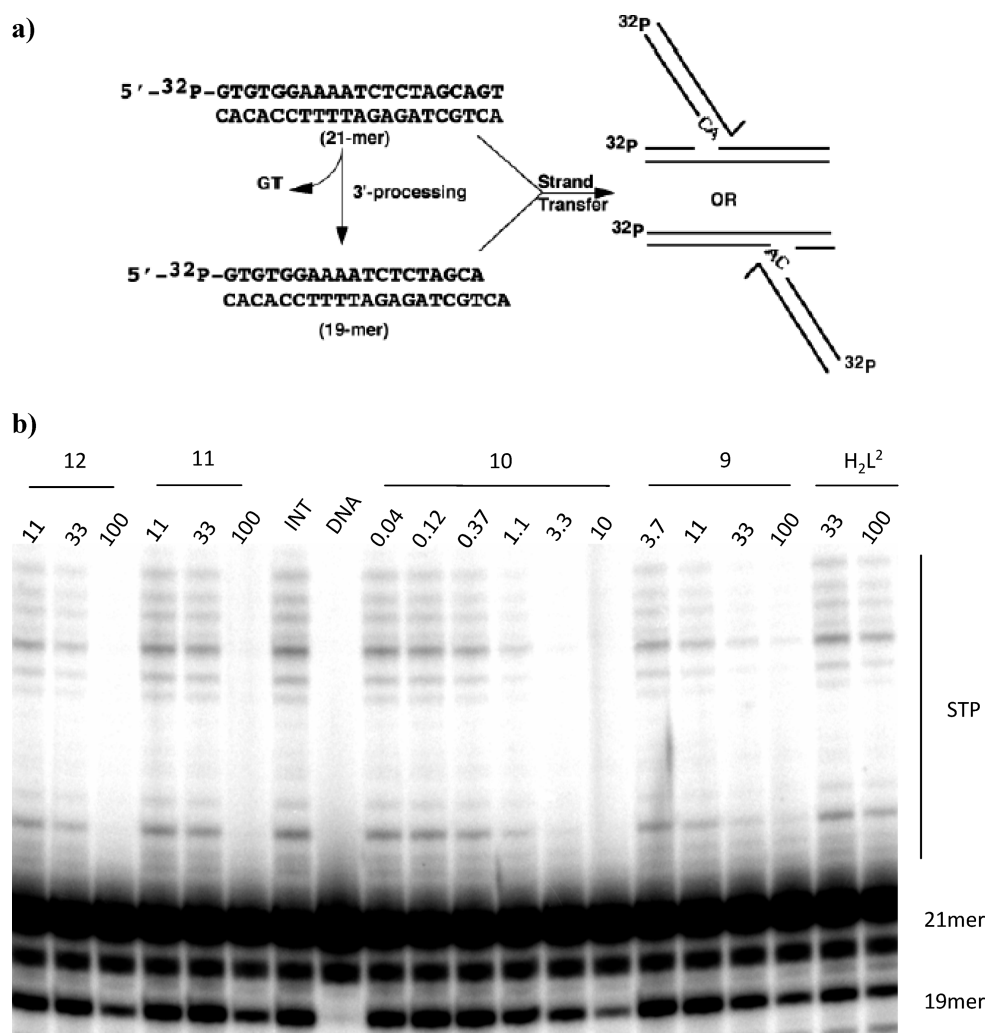


Figure 7. A representative gel showing inhibition of purified IN by selected compounds H_2L^2 and complexes 9–12. (a) A 21-mer blunt-end oligonucleotide corresponding to the U5 end of the HIV-1 LTR, 5' end-labeled with ^{32}P , is reacted with purified IN. The initial step involves nucleolytic cleavage of two bases from the 3'-end, resulting in a 19-mer oligonucleotide. Subsequently, 3' ends are covalently joined at several sites to another identical oligonucleotide that serves as the target DNA. This reaction is referred to as strand transfer, and the products formed migrate more slowly than the original substrate (shown in the Figure 6b as STP, for strand transfer products). (b) Line named as DNA indicates DNA alone; line termed INT indicates IN and DNA with no drug; other lines: IN, DNA and selected drug concentrations (μM) as indicated in each line. STP indicates strand transfer products.

X-ray Crystallography of $[Mn(HL^2)_2(CH_3OH)_2] \cdot 2CH_3OH$. Slow evaporation of a methanolic solution of **12** afforded crystals of $[Mn(HL^2)_2(CH_3OH)_2] \cdot 2CH_3OH$ suitable for X-ray diffraction. Crystals were not stable in air, probably due to the loss of crystallization solvent molecules. $[Mn(HL^2)_2(CH_3OH)_2]$ consists of a centrosymmetric molecular complex where the Mn^{2+} center is octahedrally coordinated by two monodeprotonated ligands occupying the equatorial plane in a bidentate fashion, and two apical methanol molecules. Two uncoordinated solvation methanol molecules complete the cell contents. Figure 4 shows the molecular structure and labeling of $[Mn(HL^2)_2(CH_3OH)_2] \cdot 2CH_3OH$. Deprotonation of the ligand occurs at the keto-enolic system, whose chelation on the metal originates a pentatomic ring slightly puckered in an envelope shape (Cremer and Pople⁵³ puckering coordinates: $Q_T = 0.15$, $\theta_2 = 115^\circ$). The two C–O bonds of the keto enolic system are perfectly equivalent in length, while a certain asymmetry is observed on the carbon backbone, since the C8–C9 bond is significantly shorter

than the adjacent C7–C8. The terminal rings are not coplanar with the chelation system (C8–C9–C10–N1 = 19° ; C8–C7–C1–C6 = -36°) and form a dihedral angle of 45° between them. The NH groups on the triazole rings point to the internal side of the complex, in cis position with respect to the Mn–O coordination bonds. The complex is supramolecularly associated to a pair of uncoordinated solvation methanol molecules, which are docked by $NH \cdots O$ and $CH \cdots O$ interactions with the NH of the triazole rings and the O2 of the CO groups (N3–H \cdots O4 = 2.742(4)Å, 169(3) $^\circ$; C13–H \cdots O2(i) = 3.421(3)Å, 144(1) $^\circ$; $i = -x, 1 - y, 1 - z$) (Figure 5).

It is interesting to note that, in the X-ray structure of SCITEP cocrystallized with the enzyme,¹² the inhibitor is located in the center of the active site without coordinating directly the magnesium ion, but all four nitrogen atoms of the tetrazole ring are hydrogen-bonded to the protein. The involvement of the triazole ring in extensive hydrogen bonding in the crystal structure of $[Mn(HL^2)_2(CH_3OH)_2] \cdot 2CH_3OH$ confirms the role this

moiety has in molecular recognition, even when it does not directly coordinate the metal ions. Note, also, that the OH methanol coordinated to magnesium was recently used to simulate the processed viral 3'-DNA end, ready to attack a host DNA phosphodiester bond in a theoretical study on magnesium chelation of IN inhibitors.⁵²

Potentiometric Measurements and Calculations. In order to obtain more information about the behavior of H_2L^2 in solution, a potentiometric study was carried out with Mg^{2+} and Mn^{2+} . To reduce solubility problems, the titrations were performed in methanol/water = 9/1 v/v, where all the species are soluble in the examined pH range. First, the protonation constants of the ligand were determined as $pK_{a1} = 8.226(0.008)$ and $pK_{a2} = 11.431(0.008)$; the former is attributed to the enol OH, the latter to the proton bound to the nitrogen in the heterocycle. The metal ion coordination lowers the pK_{a1} so that complexes with the monodeprotonated ligand are formed also in an acidic environment (see Figure 6). Afterward, the stoichiometry of the complexes with Mn^{2+} and Mg^{2+} were determined. 1:1 and 1:2 metal to ligand ratios have been considered, and the corresponding diagrams are shown (Figure 6 and Figure S1 in the Supporting Information). The best fit of the experimental titration curves was obtained by the set of species shown in Table 1. The species found in solution for Mn(II) ($[M(HL^2)]^+$, $M(HL^2)_2$, $[M(HL^2)L^2]^-$, ML^2 and $[ML^2(OH)]^-$) are the same for Mg(II), with similar formation constants for the two systems. This model is corroborated by very good statistical parameters and by the overlapping between experimental and computed titration curves. Dimeric models of type $M_2(\text{ligand})_2$ were also taken into account, but gave rise to a worse fitting or were rejected by calculation. However, the observation of a 1:1 species in solution is not in contrast with the isolation of dimeric complexes in solid state.

It is worth noting that Mn(II) is more efficient than Mg(II) in fully deprotonating the ligand: $[Mn(HL^2)L^2]^-$ and MnL^2 start forming at $pH \sim 6$ whereas $[Mg(HL^2)L^2]^-$ starts forming at pH around 7.5, and MgL^2 is present in very small amount in alkaline environment. Besides, the $[ML^2(OH)]^-$ species is formed in a small amount only above pH 10. As shown by the distribution diagrams in Figure 6, at a physiological pH , the species $[MHL^2]^+$ and $M(HL^2)_2$ are the most abundant for Mg(II), whereas all the species, excluding $[MnL^2(OH)]^-$, are found for Mn(II).

In conclusion, H_2L^2 behaves in a different way with respect to the previously studied DKA ligand.^{37,38} In fact, as can be seen in the distribution diagram, complexes with a 1:1 metal to ligand ratio are less stable with H_2L^2 than with the parent DKA compound H_2L^1 . Moreover, the formation constants of $M(HL^2)_2$ are much greater than for the other species in solution.

Inhibition of HIV-1 IN. The ligands H_2L^1 and H_2L^2 and their complexes **9–12** were tested for their ability to inhibit 3'-processing and strand transfer catalytic activities by oligonucleotide-based assays (Table 2 and Figure 7). Inhibition of strand transfer activities in *in vitro* assays for complexes **9–12** were also evaluated by using either Mn^{2+} and Mg^{2+} . All tested compounds showed anti-IN activity in the nanomolar/micromolar range. In particular, as far as the inhibitory activities of the ligands are concerned, H_2L^1 (IC_{50} , strand transfer = $0.5 \pm 0.3 \mu M$; 3'-processing = $9 \pm 2 \mu M$) was 100-fold more potent than H_2L^2 (IC_{50} , strand transfer = $43 \pm 7 \mu M$; 3'-processing > $100 \mu M$). H_2L^2 was about 70-fold less potent than its parent compound S-1360 ($IC_{50} = 0.6 \pm 1 \mu M$ against strand transfer);⁵⁴ it has an activity similar to the previously studied H_2L (Figure 2a)

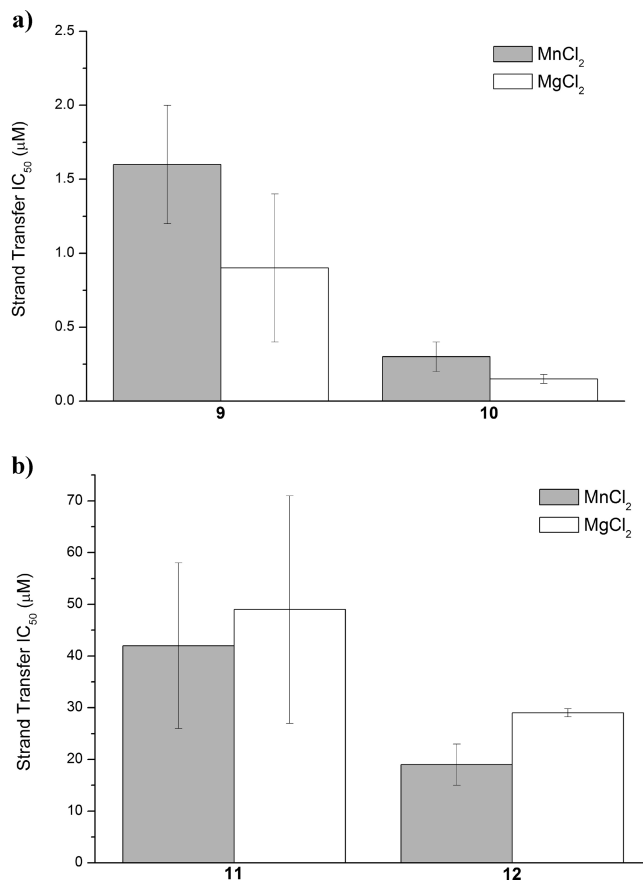


Figure 8. Comparison of inhibition of HIV-1 IN catalytic activities of complexes **9** and **10** (a) and **11** and **12** (b) using either $MnCl_2$ or $MgCl_2$ in the reaction buffer.

(IC_{50} , 3'-processing > 333 ; strand transfer = $69 \pm 4 \mu M$).³⁷ These data further confirm the fundamental role of the hydrophobic substituent of the chelating moiety, and also that the substitution of the diketo acid functionality with a triazolic ring does not affect the activity.

The complexes **9–12** retained an activity profile analogous to the corresponding free ligands (Table 2 and Figure 7), with IC_{50} values for inhibition of strand transfer ranging from 0.15 to $1.6 \mu M$ for **9** and **10**, and from 19 to $49 \mu M$ for **12** and **11**, respectively (for representative gels, see Figure 7b). Interestingly, with IC_{50} values of 0.15 ± 0.03 and $3 \pm 0.01 \mu M$ (strand transfer and 3'-processing, respectively) the manganese complex **10** proved to be the most potent compound, with 6-fold greater potency than its magnesium congener **9** ($IC_{50s} = 0.9 \pm 0.5$ and $52 \pm 18 \mu M$, for strand transfer and 3'-processing). A similar "metal dependent"^{37,55} behavior was also shown by **11** and **12**.

Complexes **9** and **10**, as well as **11** and **12**, inhibit IN in similar concentration range, when tested in the presence of either Mg or Mn ions in the reaction buffer (Figure 8). When tested in the presence of Mg ions in the reaction buffer, **9** and **10** show an increase in potency, whereas a slight decrease in inhibition activity for **11** and **12** was observed (Figure 8). These results could be related to the selectivity of the free ligands vs the metal, resulting in different equilibria in the medium. The concentration of Mg^{2+} *in vitro* and *in vivo* therefore makes plausible the hypothesis that the free ligands could also act as complexes in their active form, as they

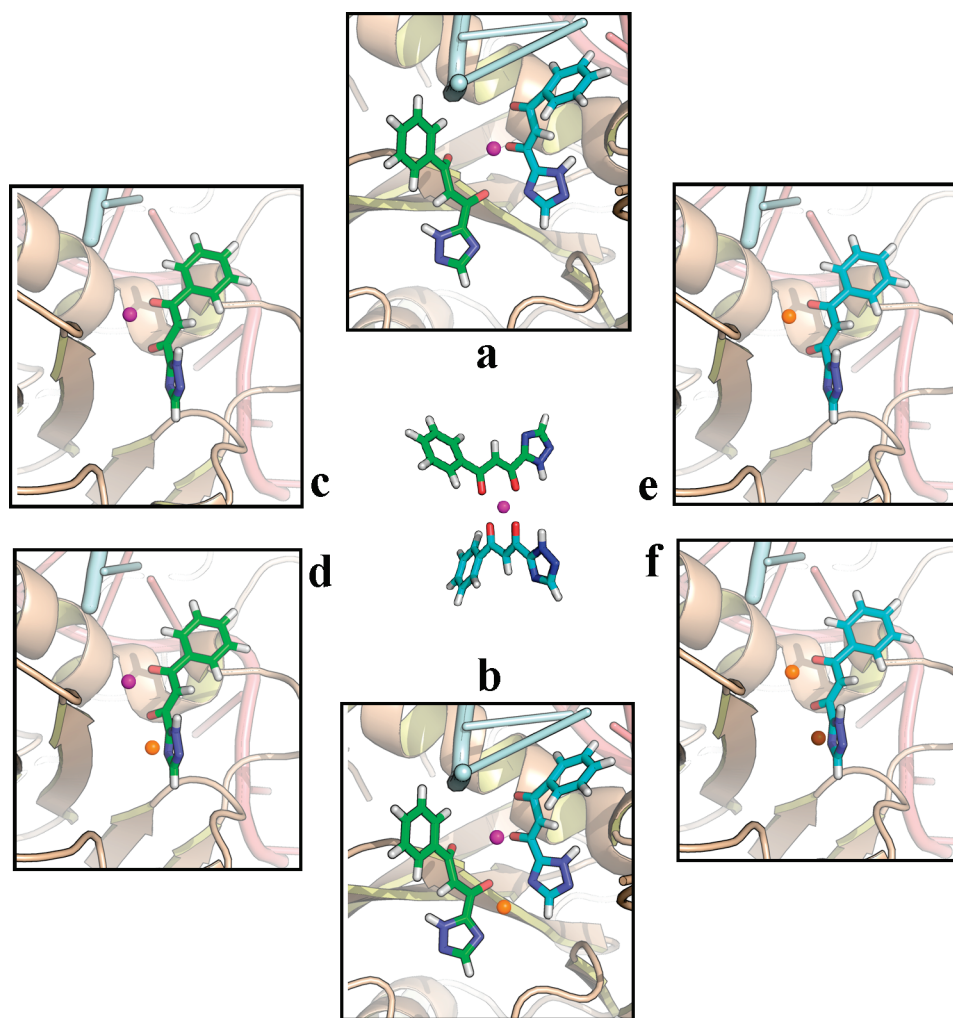


Figure 9. Metal complex ML_2 and related proposed structures highlighting the hypothetical metal binding model into the active site of the IN-DNA intasome (depicted in cartoon). Magenta spheres indicate the Mg^{2+} ions of the complex inhibitors, while the Mg^{2+} ions in the catalytic core are shown as orange spheres. Panels a–f show graphical representations of putative interactions of complexes/ligand in the IN active site. The complex ML_2 (a) or ML (c) bind directly to IN. ML_2 (b) or ML (d) interacts with IN and chelates a second ion on the active site. A complex with one (e) or two (f) metal ions in the site may be formed upon binding of ML_2 or ML to IN and subsequent dynamic exchange of the metal ions. The structure pdb.3L2Q was selected and optimized to be used as a model target. These images were prepared using the PyMOL program.

could coordinate ions in solution before interaction at their putative binding site.

If we take into consideration H_2L^2 and its complexes, it is clear from potentiometric and synthetic data that a direct involvement of the triazole in the coordination to a second metal ion would be difficult. The local conditions inside the active site could allow the deprotonation of the triazolic moiety and the coordination of a second metal ion. Otherwise, the triazolic group can establish hydrogen bonding with the protein side chain. This fact, in synergy with the complexation of one metal ion, can block the interaction between IN and the DNA substrate, in analogy with the situation found in the crystal structure of SCITEP in complex with the enzyme.¹² In other words, the reactive species could be the monometallic complex that in the intasome interacts with the second metal ion and the protein. Again, as recently observed by theoretical investigation,⁵² when a methanol molecule, which simulates the terminal 3'-OH of viral DNA, replaces a coordinated water molecule in the complex, as in $[Mn(HL^2)_2 \cdot (CH_3OH)_2] \cdot 2CH_3OH$, the metal chelation is still well established. This suggests that, in the real binding site of IN, the

terminal 3'-OH functionality may be interacting with one magnesium ion. The biological profile of complex 12, with respect to that of its free ligand H_2L^2 , seems to support this assumption.

Finally, as expected, selective strand transfer inhibition was confirmed for all tested compounds, as evidenced by their selectivity indices.

One- or Two-Metal Binding Inhibition Mechanism?. A simple molecular recognition study of the binding mode of ligand/ Mg^{2+} complexes in 1:1 and 2:1 (L:M) stoichiometric ratio on the active site of IN was performed by means of a molecular modeling docking approach. On the basis of the X-ray crystal structure of IN-DNA intasome (pdb.3L2Q), a model active site with a set of magnesium species in the IN active site was built by manual docking. Energy minimization and equilibration and visual inspection were performed by the Molecular Operating Environment (MOE) program. Trajectory and poses were sampled and visually examined by using the PyMOL program. The triazolic nitrogen of the ligand was taken as neutral, as suggested from the pK_a , even if it is known that the pK_a of several ligands can vary by about 1–1.5 units upon coordination or within enzyme active site.

A graphical representation of putative interactions of the metal complex MgL_2 and related proposed structures into the active site of the IN-DNA intasome is depicted in Figure 9 (panels a–f). Several hypotheses may be invoked. The complex ML_2 (a) or ML (c) can bind directly to IN, interacting as a complex according to an “interfacial mechanism”: the complex could act as a static entity, preventing the interaction between the enzyme and the DNA substrate, thus blocking the integration at the strand transfer stage. It is also possible that ML_2 (b) or ML (d) binds to IN and chelates a second ion that is present on the active site, giving rise to a dimer within the active site. Furthermore, a complex with one (e) or two (f) metal ions in the site may be formed upon binding of ML_2 or ML to IN and subsequent dynamic exchange of the metal ions (Figure 9).

CONCLUSIONS AND PERSPECTIVES

The present study focuses on H_2L^1 and H_2L^2 , two DKA HIV-1 IN inhibitors, and, in particular, on their Mg^{2+} and Mn^{2+} complexes, with the aim to elucidate at the molecular level some important mechanistic aspects that could be extended to the chelating inhibitors in general. By comparing the spectroscopic, potentiometric and structural data, it is clear that the diketo acid functionality chelates divalent metal ions, forming complexes with metals in different stoichiometric ratios. Moreover, analysis of the biological results suggests that these compounds can also act as complexes in their active form. Moreover, the electronic properties of the aromatic framework influence the metal-chelating ability of the pharmacophore and, consequently, the activity. Therefore, the difference in activities may be related to the complexes they preferentially form in solution.

Another relevant point that emerges from this study is that H_2L^2 preferentially chelates only one metal ion through the keto–enol fragment, while the triazolic moiety is excluded by coordination at least at normal physiological conditions. This is confirmed by spectroscopic and potentiometric measurements and by X-ray diffraction analysis on $[Mn(HL^2)_2(CH_3OH)_2] \cdot 2CH_3OH$. However, the triazolic moiety is involved in a complex web of hydrogen bonds both in the structure of the ligand and in the structure of the Mn^{2+} complex; in analogy, it could be involved in extensive interactions with IN and/or DNA. Therefore, at least for this ligand, a two-metal binding model could be reformulated: inhibition of IN by DKA-like inhibitors strictly requires the chelation of at least one metal ion within the catalytic core. It can be thought that the selectivity displayed by DKAs for strand transfer could not derive by the fact that inhibitors need both metal ions to bind strongly to the enzyme. It is plausible that chelation involves, in the first instance, only one metal and that binding of the inhibitor to the protein is possible only after the conformational changes occurring with 3'-processing, which would allow the accommodation of the ligand within the catalytic core. This would also explain the importance of the aromatic substituents of the inhibitors, since the hydrophobic portion is fundamental in orientating the drug within the protein active site.

We expect that the structural insights obtained from this study can be useful to look at the “two metal chelation” model in a larger context, where, together with coordination, hydrogen bonding and hydrophobic interactions should be considered as a whole.

EXPERIMENTAL SECTION

Materials and Methods. Anhydrous solvents and all reagents were purchased from Sigma-Aldrich, Merck or Carlo Erba and used without further purification. All reactions involving air- or moisture-sensitive compounds were performed under a nitrogen atmosphere using oven-dried glassware and syringes to transfer solutions. Melting points (mp) were determined using an Electrothermal melting point or a Kofler apparatus and are uncorrected. Analytical thin-layer chromatography (TLC) was carried out on Merck silica gel F-254 plates. Flash chromatography purifications were performed on Merck silica gel 60 (230–400 mesh ASTM) as the stationary phase.

NMR spectra were recorded at 27 °C on a Bruker Avance 300 FT and Varian XL-200 spectrophotometers by using $SiMe_4$ as internal standard; the assignment of exchangeable protons (OH and NH) was confirmed by the addition of D_2O . IR spectra were obtained with a Nicolet SPCFT-IR spectrophotometer in the 4000–400 cm^{-1} range, in reflectance mode on the powder. Elemental analyses were performed by using a Carlo Erba Model EA 1108 apparatus. The ESI(+)-MS spectra were collected by using a quadrupole-time-of-flight micro mass spectrometer (Micro-mass, Manchester, U.K.) equipped with a pneumatically assisted ESI interface. The system was controlled by Masslynx software version 4.0 (Micromass). The nebulizing gas (nitrogen, 99.999% purity) and the desolvation gas (nitrogen, 99.998% purity) were delivered at a flow-rate of 10 and 600 L/h respectively. Continuum mode full-scan mass spectra were acquired using an acquisition time of 1 s and an interscan delay of 0.1 s. QqTOF external calibration was performed using a 0.1% phosphoric acid solution and a fifth-order nonlinear calibration curve was usually adopted.

Intermediates 5–7 were prepared using the starting material 3 and 4 as previously described.⁴⁸

Methyl 4-(3,5-Bis(benzyloxy)phenyl)-2-hydroxy-4-oxobut-2-enoate (2). To a solution of 3,5-dibenzyloxy-acetophenone (**1**, 8.3 mmol) and dimethyl oxalate (10.0 mmol) in DMF (10 mL), NaH (60% oil dispersion, 10.0 mmol) was added at 5 °C. The reaction mixture was stirred at rt for 3.5 h and then heated at 50 °C for 1 h. After cooling in an ice-bath, the reaction was quenched with water and acidified with 3 N HCl. The precipitate was filtered and washed several times with water to afford a white powder corresponding to a mixture of the Z/E isomers (6:1). Yield: 73%. Mp: 91–92 °C [lit. 121–123 °C, for E-isomer].⁴⁷ IR (cm^{-1}): $\nu_{C=O_{ester}}$ 1725, $\nu_{C=O_{keto}}$ 1625. ¹H NMR (DMSO-*d*₆) for the Z-isomer: δ 7.48–7.34 (m, 10H, Ar-H), 7.27 (s, 2H, Ar-H), 7.14 (s, 1H, Ar-H), 7.01 (s, 1H, CH), 5.19 (s, 4H, CH₂), 3.86 (s, 3H, OCH₃). ESI/MS (+, *m/z*): 418 [M^+]. Anal. Calcd for C₂₅H₂₂O₆: C 71.75; H 5.30. Found: C 71.68; H 5.61.

(Z)-4-(3,5-Bis(benzyloxy)phenyl)-2-hydroxy-4-oxobut-2-enoic Acid (H_2L^1). To a solution of **2** (1.0 mmol) in methanol (15 mL), 2 N NaOH (4.0 mmol) was added. The resulting mixture was vigorously stirred for 5 h. After dilution with water, the reaction mixture was acidified with 1 N HCl. The white-beige precipitate was filtered off, washed with water, and recrystallized from hexane/ethyl acetate to give a pale yellow powder. Yield: 85%. Mp: 171 °C [lit. 170–172 °C].²⁵ IR (cm^{-1}): $\nu_{C=O_{acid}}$ 1707, $\nu_{C=O_{keto}}$ 1623. ¹H NMR (DMSO-*d*₆): δ 7.49–7.30 (m, 10H, Ar-H), 7.26 (d, 2H, Ar-H), 7.09 (s, 1H, Ar-H), 7.00 (s, 1H, CH), 5.19 (s, 4H, CH₂). ESI/MS (+, *m/z*): 404 [M^+]. Anal. Calcd for C₂₄H₂₀O₆: C 71.26; H 4.99. Found: C 71.00; H 5.07.

Synthesis of (Z)-3-Hydroxy-1-phenyl-3-(1-trityl-1H-1,2,4-triazol-5-yl)prop-2-en-1-one (8). A 1 M solution of LiHMDS in THF (3.87 mmol) was added at $-70\text{ }^{\circ}\text{C}$ to a solution of acetophenone (2.98 mmol) in THF (9 mL) under a nitrogen atmosphere. The reaction mixture was slowly warmed to $-10\text{ }^{\circ}\text{C}$ and cooled to $-70\text{ }^{\circ}\text{C}$. 7 (3.87 mmol) in THF (15 mL) was added, and the reaction mixture was slowly warmed to rt and stirred at the same temperature for 1.5 h. The reaction was quenched with a 10% aqueous solution of NH_4Cl and was acidified with 3 N HCl. The solution was extracted with ethyl acetate and the combined organic layers were washed with brine and dried over sodium sulfate, filtered and the solvent removed *in vacuo* to give an orange solid that was triturated from diethyl ether to afford a pale orange solid. Yield: 89%. Mp: 169–171 $^{\circ}\text{C}$ (dec). IR (cm^{-1}): $\nu_{\text{C}=\text{O}_{\text{carbonyl}}}$ 1615. ^1H NMR ($\text{DMSO}-d_6$): δ 14.60–14.20 (s, br, 1H, OH), 8.31 (s, 1H, CH), 8.02 (d, 2H, Ar–H), 7.70–7.25 (m, 12H, Ar–H), 7.22 (s, 1H, COCH), 7.20–6.92 (m, 7H, Ar–H). ESI/MS (+, m/z): 457 [M^+].

Synthesis of (Z)-3-Hydroxy-1-phenyl-3-(1H-1,2,4-triazol-3-yl)prop-2-en-1-one (H_2L^2). 3 N HCl (7.8 mL) was added to a solution of compound 8 (2.34 mmol) in 1,4-dioxane (30 mL), and the mixture was stirred at $80\text{ }^{\circ}\text{C}$ for 30 min. Then, the reaction was cooled to rt and the solvent was evaporated *in vacuo* to give a residue, which was dissolved in diethyl ether and extracted with 1 N NaOH. The combined aqueous layers were acidified with 3 N HCl, and the precipitate formed was filtered and washed with water and ethyl acetate. The solid residue was crystallized from ethyl acetate to afford a yellow solid. Yield: 85%. Mp: 197–198 $^{\circ}\text{C}$ (dec). IR (cm^{-1}): $\nu_{\text{C}=\text{O}}$ 3580, $\nu_{\text{C}=\text{O}_{\text{carbonyl}}}$ 1610, $\nu_{\text{C}=\text{C}}$ 1573. ^1H NMR ($\text{DMSO}-d_6$): δ 14.80–14.60 (s, br, 1H, OH), 8.73 (s, br, 1H, CH), 8.07–7.97 (m, 2H, Ar–H), 7.71–7.51 (m, 3H, Ar–H), 7.28 (s, 1H, COCH), 4.80 (CH_2 , keto isomer). ESI/MS (+, m/z): 215 [M^+]. Anal. Calcd for $\text{C}_{11}\text{H}_9\text{N}_3\text{O}_2 \cdot 0.25\text{H}_2\text{O}$: C 60.13; H 4.35; N 19.11. Found: C 59.86; H 4.04; N 18.85.

$\text{Mg}_2\text{L}_2^1 \cdot 5\text{H}_2\text{O}$ (9). Ligand H_2L^1 (100 mg, 0.2 mmol) was dissolved in 20 mL of warm methanol and the pH adjusted to 7 by using NaOH 1 M. $\text{Mg}(\text{OH})_2$ (14 mg, 0.2 mmol) was added, and the reaction mixture was stirred for 24 h at room temperature. On concentrating the solution, a light yellow precipitate appeared, which was filtered off and washed with water. IR (cm^{-1}): ν_{OH} = 3695; $\nu_{\text{C}=\text{O}}$ = 1594, 1373. ^1H NMR ($\text{DMSO}-d_6$): δ 7.47–7.31 (m, 11H, Ar–H); 7.17 (s, 2H, Ar–H), 6.96 (s, 1H, $\text{CH}_{\text{enolic}}$); 5.16 (s, 4H, OCH_2). Anal. Calcd for $\text{C}_{48}\text{H}_{36}\text{Mg}_2\text{O}_{12} \cdot 5\text{H}_2\text{O}$: C 61.43; H 4.94. Found: C 61.37; H 5.51.

$\text{Mn}_2\text{L}_2^1 \cdot \text{H}_2\text{O}$ (10). Ligand H_2L^1 (100 mg, 0.2 mmol) was dissolved in 20 mL of warm methanol and added to an aqueous solution of $\text{Mn}(\text{CH}_3\text{COO})_2$ (60 mg, 0.2 mmol). Immediately, a yellow-brown precipitate was formed, which was stirred for additional 4 h, filtered off and washed with water. IR (cm^{-1}): $\nu_{\text{C}=\text{O}}$ = 1575, 1341. Anal. Calcd for $\text{C}_{48}\text{H}_{36}\text{Mn}_2\text{O}_{12} \cdot \text{H}_2\text{O}$: C 61.81; H 4.10. Found: C 61.79; H 4.10.

$\text{Mg}(\text{HL}^2)_2 \cdot 4\text{H}_2\text{O}$ (11). Ligand H_2L^2 (150 mg, 0.7 mmol) was dissolved in 20 mL of methanol and the pH adjusted to 8 by using 1 M KOH. An aqueous solution of MgCl_2 (0.35 mmol) was added, and a white precipitate appeared. The reaction mixture was stirred at room temperature for 2 h, and the precipitate was filtered off and washed with water. IR (cm^{-1}): ν_{OH} = 3640; ν_{NH} = 3422; $\nu_{\text{C}=\text{O}}$ = 1597, 1540, 1426. ^1H NMR ($\text{DMSO}-d_6$): δ 14.30 (s, br, 1H, NH), 8.21 (s, br, 1H, CH); 7.91 (d, 2H, H_{arom}); 7.44 (m, 3H, H_{arom}), 6.94 (s, 1H, $\text{CH}_{\text{enolic}}$). Anal. Calcd

for $\text{C}_{22}\text{H}_{16}\text{MgN}_6\text{O}_4 \cdot 4\text{H}_2\text{O}$: C 50.36, H 4.61, N 16.00. Found: C 50.48; H 4.35; N 15.78. ESI/MS (+, m/z): 453 [MH^+].

$\text{Mn}(\text{HL}^2)_2 \cdot 4\text{H}_2\text{O}$ (12). The same as $\text{Mg}(\text{HL}^2)_2$, by using $\text{Mn}(\text{CH}_3\text{COO})_2$. A yellow precipitate was formed, which was filtered off and washed with water/diethyl ether. IR (cm^{-1}): ν_{NH} = 3397; $\nu_{\text{C}=\text{O}}$ = 1598, 1569, 1417. Anal. Calcd for $\text{C}_{22}\text{H}_{16}\text{MnN}_6\text{O}_4 \cdot 4\text{H}_2\text{O}$: C 47.61; H 4.35; N 15.13. Found: C 47.92; H 4.17; N 15.09. ESI/MS (+, m/z): 484 [MH^+].

$\text{Mg}_2\text{L}^2 \cdot 5\text{H}_2\text{O}$ (13). Ligand H_2L^2 (100 mg, 0.47 mmol) was dissolved in 15 mL of methanol, and KOH 1 M was added until pH 10 was reached. $\text{Mg}(\text{CH}_3\text{COO})_2$ (1 equiv) dissolved in 2 mL of water was added at room temperature. After a few minutes, a white precipitate was formed, which was stirred at room temperature for 2 h. It was then filtered off and washed with water. IR (cm^{-1}): ν_{OH} = 3420; $\nu_{\text{C}=\text{O}}$ = 1605, 1571, 1527. ^1H NMR ($\text{DMSO}-d_6$): δ 8.18–7.93 (br, 3H, CH + H_{arom}); 7.54 (br, 3H, H_{arom}); 6.99 (s, 1H, $\text{CH}_{\text{enolic}}$). Anal. Calcd for $\text{C}_{22}\text{H}_{14}\text{Mg}_2\text{N}_6\text{O}_4 \cdot 5\text{H}_2\text{O}$: C 46.82; H 4.28; N 14.88. Found: C 47.08; H 4.10; N 14.57. ESI/MS (+, m/z): 475 [MH^+].

X-ray Crystallography. Crystals of $\text{H}_2\text{L}^2 \cdot (1/2)\text{HCl}$ suitable for X-ray diffraction were obtained by slow evaporation of a methanol/HCl solution of the ligand. Data were processed by Lorentz and polarization corrections for $\text{H}_2\text{L}^2 \cdot (1/2)\text{HCl}$, and by the SAINT package,⁵⁶ corrected for absorption effects by the SADABS⁵⁷ procedure ($T_{\text{max}}/T_{\text{min}} = 1.000/0.699$), data reduction performed up to $d = 0.90\text{ \AA}$, for $[\text{Mn}(\text{HL})_2(\text{CH}_3\text{OH})_2] \cdot 2\text{CH}_3\text{OH}$. The phase problem was solved by direct methods⁵⁸ and refined by full matrix least-squares on all F^2 . Anisotropic displacement parameters⁵⁹ were refined for all non-hydrogen atoms, while hydrogen atoms were located from difference Fourier maps; methanol hydrogens were introduced in idealized positions. The final maps were featureless. For the discussion use was made of the Cambridge Structural database facilities.⁶⁰

Potentiometric Measurements. The metal ions stock solutions were prepared from $\text{MnCl}_2 \cdot 4\text{H}_2\text{O}$ (Janssen) and $\text{MgCl}_2 \cdot 6\text{H}_2\text{O}$ (Aldrich). Their concentrations were determined by using EDTA as a titrant. The sodium salt of Eriochrome black T in the presence of triethanolamine and hydroxylamine chloride for Mn(II) and Mg(II) was used as an indicator. Equilibrium constants for protonation and complexation reactions were determined by means of potentiometric measurements, carried out in methanol/water = 9:1 v/v solution at ionic strength 0.1 M KCl and $25 \pm 0.1\text{ }^{\circ}\text{C}$, in the pH range 2.5–11 under N_2 . Temperature was controlled to $\pm 0.1\text{ }^{\circ}\text{C}$ by using a thermostatic circulating water bath (ISCO GTR 2000 Iix). Appropriate aliquots of ligand solution, prepared by weight, were titrated with standard KOH (solvent: methanol/water = 9:1 v/v, $I = 0.1\text{ M}$ KCl) with and without metal ions, applying constant-speed magnetic stirring. Freshly boiled methanol and bidistilled water, kept under N_2 , were used throughout. The experimental procedure in order to reach very high accuracy in the determination of the equilibrium constants in this mixed solvent has been described in detail elsewhere.⁶¹ The protonation constants of the ligands were obtained by titrating 20–50 mL samples of each ligand (1×10^{-3} to $3 \times 10^{-3}\text{ M}$). For the complex formation constants, the titrations were performed with different ligand/metal ratios (1 up to 4). At least two measurements (about 60 experimental points each) were performed for each system. Potentiometric titrations were carried out by a fully automated apparatus equipped with a CRISON GLP 21-22 digital voltmeter (resolution 0.1 mV) and a 5 mL Metrohm Dosimat 655 autoburet,

both controlled by a homemade software in BASIC, working on an IBM computer. The electrodic chain (Crison 5250 glass electrode and KCl 0.1 M in methanol/water = 9:1 v/v calomel electrode, Radiometer 401) was calibrated in terms of $[H^+]$ by means of a strong acid–strong base titration, by Gran's method,⁶² allowing the determination of the standard potential, E° (372.5 ± 0.4 mV), and of the ionic product of water, K_w ($pK_w = 14.40 \pm 0.05$) in the experimental conditions used. The software HYPERQUAD⁶³ was used to evaluate the protonation and complexation constants from emf data.

Biological Materials, Chemicals, and Enzymes. All compounds were dissolved in DMSO, and the stock solutions were stored at -20°C . The γ [³²P]-ATP was purchased from Perkin-Elmer. The expression system for wild-type IN was a generous gift of Dr. Robert Craigie, Laboratory of Molecular Biology, NIDDK, NIH, Bethesda, MD.

Preparation of Oligonucleotide Substrates. The oligonucleotides 21top, 5'-GTGTGGAAAATCTCTAGCAGT-3', and 21bot, 5'-ACTGCTAGAGATTTTCCACAC-3', were purchased from Norris Cancer Center Core Facility (University of Southern California) and purified by UV shadowing on polyacrylamide gel. To analyze the extent of 3'-processing and strand transfer using 5'-end labeled substrates, 21top was 5'-end labeled using T₄ polynucleotide kinase (Epicenter, Madison, WI) and γ [³²P]-ATP (Amersham Biosciences or ICN). The kinase was heat-inactivated, and 21bot was added in 1.5 molar excess. The mixture was heated at 95°C , allowed to cool slowly to room temperature, and run through a spin 25 minicolumn (USA Scientific) to separate annealed double-stranded oligonucleotide from unincorporated material.

Integrase Assays. To determine the extent of 3'-processing and strand transfer, wild-type IN was preincubated at a final concentration of 200 nM with the inhibitor in reaction buffer (50 mM NaCl, 1 mM HEPES, pH 7.5, 50 μM EDTA, 50 μM dithiothreitol, 10% glycerol (w/v), 7.5 mM MnCl₂, 0.1 mg/mL bovine serum albumin, 10 mM 2-mercaptoethanol, 10% DMSO, and 25 mM MOPS, pH 7.2) at 30°C for 30 min. Then, 20 nM of the 5'-end ³²P-labeled linear oligonucleotide substrate was added, and incubation was continued for an additional 1 h. Reactions were quenched by the addition of an equal volume (16 μL) of loading dye (98% deionized formamide, 10 mM EDTA, 0.025% xylene cyanol and 0.025% bromophenol blue). An aliquot (5 μL) was electrophoresed on a denaturing 20% polyacrylamide gel (0.09 M tris-borate pH 8.3, 2 mM EDTA, 20% acrylamide, 8 M urea).

Gels were dried, exposed in a PhosphorImager cassette, analyzed using a Typhoon 8610 Variable Mode Imager (Amersham Biosciences) and quantitated using ImageQuant 5.2. Percent inhibition (% I) was calculated using the following equation:

$$\% I = 100 \times [1 - (D - C)/(N - C)]$$

where C , N , and D are the fractions of 21-mer substrate converted to 19-mer (3'-processing product) or ST products for DNA alone, DNA plus IN, and IN plus drug, respectively. The IC_{50} values were determined by plotting the logarithm of drug concentration versus percent inhibition to obtain concentration that produced 50% inhibition.

■ ASSOCIATED CONTENT

● **Supporting Information.** Distribution diagrams for magnesium and manganese complexes with H_2L^2 and ligand:M ratio

1:1. X-ray diffraction analysis for $H_2L^2 \cdot (1/2)HCl$ and complex $[Mn(HL^2)_2(CH_3OH)_2] \cdot 2CH_3OH$ with crystal data, structure refinement, and most relevant bond lengths and angles. This material is available free of charge via the Internet at <http://pubs.acs.org>. Crystallographic data (excluding structure factors) for $H_2L^2 \cdot (1/2)HCl$ and $[Mn(HL^2)_2(CH_3OH)_2] \cdot 2CH_3OH$ have been deposited with the Cambridge Crystallographic Data Centre as supplementary publications nos. CCDC 791917–791918. Copies of the data can be obtained free of charge on application to CCDC, 12 Union Road, Cambridge CB2 1EZ, U.K. (fax: (+44) 1223-336-033; e-mail: deposit@ccdc.cam.ac.uk).

■ AUTHOR INFORMATION

Corresponding Author

*University of Parma, Dipartimento di Chimica Generale ed Inorganica, Chimica Analitica, Chimica Fisica, Viale delle Scienze 17/A, 43124 Parma, Italy. Phone: +39 0521-905-424. Fax: +39 0521-905-557. E-mail: dominga.rogolino@unipr.it.

■ ACKNOWLEDGMENT

The authors thank the “Centro Interfacoltà Misure Giuseppe Casnati” and the “Laboratorio di Strutturistica Mario Nardelli” of the University of Parma for facilities and Giuseppe Foroni for technical assistance. M.S. is grateful to Fondazione Banco di Sardegna for its partial financial support and to Dr. Andrea Brancale for the use of the MOE program. The work in N.N.'s laboratory was supported by funds from the Campbell Foundation.

■ ABBREVIATIONS USED

HIV-1, human immunodeficiency virus type 1; IN, integrase; ST, strand transfer; DKA, diketo acid; S-1360, (2Z)-1-[5-(4-fluorobenzyl)-2-furyl]-3-hydroxy-3-(1H-1,2,4-triazol-5-yl)prop-2-en-1-one; CSD, Cambridge Structural Database; LiHMDS, lithium bis(trimethylsilyl)amide.

■ REFERENCES

- (1) Pommier, Y.; Johnson, A. A.; Marchand, C. Integrase inhibitors to treat HIV/AIDS. *Nat. Rev. Drug Discovery* **2005**, *4*, 236–248.
- (2) Neamati, N.; Marchand, C.; Pommier, Y. HIV-1 integrase inhibitors: past, present, and future. *Adv. Pharmacol.* **2000**, *49*, 147–165.
- (3) D'Angelo, J.; Mouscadet, J. F.; Desmaele, D.; Zouhiri, F.; Leh, H. HIV-1 integrase: the next target for AIDS therapy?. *Pathol. Biol.* **2001**, *49*, 237–246.
- (4) Neamati, N. Structure-based HIV-1 inhibitor design: a future perspective. *Expert Opin. Invest. Drugs* **2001**, *10*, 281–296.
- (5) Anthony, N. J. HIV-1 integrase: a target for new AIDS chemotherapeutics. *Curr. Top. Med. Chem.* **2004**, *4*, 979–990.
- (6) Nair, V.; Chi, G. HIV integrase inhibitors as therapeutic agents in AIDS. *Rev. Med. Virol.* **2007**, *17*, 277–295.
- (7) Dayam, R.; Al-Mawsawi, L. Q.; Neamati, N. HIV-1 Integrase Inhibitors: An Emerging Clinical Reality. *Drugs R&D* **2007**, *8*, 155–168.
- (8) MK-0518 meeting transcript. Department of Health and Human Services; Food and Drug Administration; Center for Drug Evaluation and Research; Antiviral Drugs Advisory Committee; 2007 September 5. Available from www.fda.gov/ohrms/dockets/ac/cder07.htm#AntiviralDrugs.
- (9) Al-Mawsawi, L. Q.; Al-Safi, R. I.; Neamati, N. *Expert. Opin. Emerging Drugs* **2008**, *13*, 213–225.
- (10) Kulkosky, J.; Jones, K. S.; Katz, R. A.; Mack, J. P.; Skalka, A. M. Residues critical for retroviral integrative recombination in a region that is highly conserved among retroviral/retrotransposon integrases and

bacterial insertion sequence transposases. *Mol. Cell. Biol.* **1992**, *12*, 2331–2338.

(11) Hazuda, D. J.; Felock, P.; Witmer, M.; Wolfe, A.; Stillmock, K.; Grobler, J. A.; Espeseth, A.; Gabryelski, L.; Schleif, W.; Blau, C.; Miller, M. D. Inhibitors of strand transfer that prevent integration and inhibit HIV-1 replication in cells. *Science* **2000**, *287*, 646–50.

(12) Goldgur, Y.; Craigie, R.; Cohen, G. H.; Fujiwara, T.; Yoshinaga, T.; Fujishita, T.; Sugimoto, H.; Endo, T.; Murai, H.; Davies, D. R. Structure of the HIV-1 integrase catalytic domain complexed with an inhibitor: a platform for antiviral drug design. *Proc. Natl. Acad. Sci. U.S.A.* **1999**, *96*, 13040–13043.

(13) Pais, G. C. G.; Burke, T. R. Novel aryl diketo-containing inhibitors of HIV-1 integrase. *Drugs Future* **2002**, *27*, 1101–1111.

(14) Egbertson, M. S. HIV integrase inhibitors: from diketoacids to heterocyclic templates: a history of HIV integrase medicinal chemistry at Merck West Point and Merck Rome (IRBM). *Curr. Top. Med. Chem.* **2007**, *7*, 1251–1272.

(15) Wang, Y.; Serradell, N.; Bolos, J.; Rosa, E. MK-0518, HIV integrase inhibitor. *Drugs Future* **2007**, *32*, 118–122.

(16) Rowley, M. The Discovery of Raltegravir, An Integrase Inhibitor for the Treatment of HIV Infection. *Prog. Med. Chem.* **2008**, *46*, 1–28.

(17) Summa, V.; Petrocchi, A.; Bonelli, F.; Crescenzi, B.; Donghi, M.; Ferrara, M.; Fiore, F.; Gardelli, C.; Gonzalez, P. O.; Hazuda, D. J.; Jones, P.; Kinzel, O.; Laufer, R.; Monteagudo, E.; Muraglia, E.; Nizi, E.; Orvieto, F.; Pace, P.; Pescatore, G.; Scarpelli, R.; Stillmock, K.; Witmer, M. V.; Rowley, M. Discovery of raltegravir, a potent, selective orally bioavailable HIV-integrase inhibitor for the treatment of HIV-AIDS infection. *J. Med. Chem.* **2008**, *51*, 5843–5855.

(18) Sato, M.; Motomura, T.; H. Aramaki, H.; Matsuda, T.; Yamashita, M.; Ito, Y.; Kawakami, H.; Matsuzaki, Y.; Watanabe, W.; Yamataka, K.; Ikeda, S.; Kodama, E.; Matsuoka, M.; Shinkai, H. Novel HIV-1 Integrase Inhibitors Derived from Quinolone Antibiotics. *J. Med. Chem.* **2006**, *49*, 1506–1508.

(19) Dayam, R.; Al-Mawsawi, L. Q.; Zawahir, Z.; Witvrouw, M.; Debyser, Z.; Neamati, N. Quinolone 3-Carboxylic Acid Pharmacophore: Design of Second Generation HIV-1 Integrase Inhibitors. *J. Med. Chem.* **2008**, *51*, 1136–1144.

(20) Di Santo, R.; Costi, R.; Roux, A.; Artico, M.; Lavecchia, A.; Marinelli, L.; Novellino, E.; Palmisano, L.; Andreotti, M.; Amici, R.; Galluzzo, C. M.; Nencioni, L.; Palamara, A. T.; Pommier, Y.; Marchand, C. Novel Bifunctional Quinolonyl Diketo Acid Derivatives as HIV-1 Integrase Inhibitors: Design, Synthesis, Biological Activities, and Mechanism of Action. *J. Med. Chem.* **2006**, *49*, 1939–1945.

(21) Pasquini, S.; Mugnaini, C.; Tintori, C.; Botta, M.; Trejos, A.; Arvela, R. K.; Larhed, M.; Witvrouw, M.; Michiels, M.; Christ, F.; Debyser, Z.; Corelli, F. Investigations on the 4-Quinolone-3-carboxylic Acid Motif. 1. Synthesis and Structure-Activity Relationship of a Class of Human Immunodeficiency Virus type 1 Integrase Inhibitors. *J. Med. Chem.* **2008**, *51*, 5125–5129.

(22) Hare, S.; Gupta, S. S.; Valkov, E.; Engelman, A.; Cherepanov, P. Retroviral intasome assembly and inhibition of DNA strand transfer. *Nature* **2010**, *464*, 232–236.

(23) Hazuda, D. J.; Anthony, N. J.; Gomez, R. P.; Jolly, S. M.; Wai, J. S.; Zhuang, L.; Fisher, T. E.; Embrey, M.; Guare, J. P., Jr.; Egbertson, M. S.; Vacca, J. P.; Huff, J. R.; Felock, P. J.; Witmer, M. V.; Stillmock, K. A.; Danovich, R.; Grobler, J.; Miller, M. D.; Espeseth, A. S.; Jin, L.; Chen, I.-W.; Lin, J. H.; Kassahun, K.; Ellis, J. D.; Wong, B. K.; Xu, W.; Pearson, P. G.; Schleif, W. A.; Cortese, R.; Emini, E.; Summa, V.; Holloway, M. K.; Young, S. D. A naphthyridine carboxamide provides evidence for discordant resistance between mechanistically identical inhibitors of HIV-1 integrase. *Proc. Natl. Acad. Sci. U.S.A.* **2004**, *101*, 11233–11238.

(24) Dayam, R.; Neamati, N. Active site binding modes of the beta-diketoacids: a multi-active site approach in HIV-1 integrase inhibitor design. *Bioorg. Med. Chem.* **2004**, *12*, 6371–6381.

(25) Pais, G. C. G.; Zhang, X.; Marchand, C.; Neamati, N.; Cowansage, K.; Svarovskaia, E. S.; Pathak, V. K.; Tang, Y.; Nicklaus, M.;

Pommier, Y.; Burke, T. R., Jr. Structure Activity of 3-Aryl-1,3-diketo-containing compounds as HIV-1 Integrase inhibitors. *J. Med. Chem.* **2002**, *45*, 3184–3194.

(26) Zhao, X. Z.; Maddali, K.; Vu, B. C.; Marchand, C.; Hughes, S. H.; Pommier, Y.; Burke, T. R., Jr. Examination of halogen substituent effects on HIV-1 integrase inhibitors derived from 2,3-dihydro-6,7-dihydroxy-1H-isoindol-1-ones and 4,5-dihydroxy-1H-isoindole-1,3(2H)-diones. *Bioorg. Med. Chem. Lett.* **2009**, *19*, 2714–2717.

(27) Kirschberg, T.; Parrish, J. Metal chelators as antiviral agents. *Curr. Opin. Drug Discovery* **2007**, *10*, 460–472.

(28) Shaw-Reid, C. A.; Munshi, V.; Graham, P.; Wolfe, A.; Witmer, M.; Danzeisen, R.; Olsen, D. B.; Carroll, S. S.; Embrey, M.; Wai, J. S.; Miller, M. D.; Cole, J. L.; Hazuda, D. J. Inhibition of HIV-1 Ribonuclease H by a Novel Diketo Acid, 4-[5-(Benzoylamino)thien-2-yl]-2,4-dioxo-butanoic Acid. *J. Biol. Chem.* **2003**, *278*, 2777–2780.

(29) Tramontano, E.; Esposito, F.; Badas, R.; Di Santo, R.; Costi, R.; La Colla, P. 6-[1-(4-Fluorophenyl)methyl-1H-pyrrol-2-yl]-2,4-dioxo-5-hexenoic acid ethyl ester a novel diketo acid derivative which selectively inhibits the HIV-1 viral replication in cell culture and the ribonuclease H activity in vitro. *Antiviral Res.* **2005**, *65*, 117–124.

(30) Billamboz, M.; Bailly, F.; Barreca, M. L.; De Luca, L.; Mouscadet, J.-F.; Calmels, C.; Andreola, M.-L.; Witvrouw, M.; Christ, F.; Debyser, Z.; Cotelle, P. Design, synthesis, and biological evaluation of a series of 2-hydroxyisoquinoline-1,3(2H,4H)-diones as dual inhibitors of human immunodeficiency virus type 1 integrase and the reverse transcriptase RNase H domain. *J. Med. Chem.* **2008**, *51*, 7717–7730.

(31) Wang, Z.; Tang, J.; Salomon, C. E.; Dreis, C. D.; Vince, R. Pharmacophore and structure–activity relationships of integrase inhibition within a dual inhibitor scaffold of HIV reverse transcriptase and Integrase. *Bioorg. Med. Chem.* **2010**, *18*, 4202–4211.

(32) Kijama, R.; Kawasuji, T. *PCT Int. Appl.* 2001, WO-01/95905.

(33) Kawasuji, T.; Fuji, M.; Yoshinaga, T.; Sato, A.; Fujiwara, T.; Kiyama, R. A platform for designing HIV integrase inhibitors. Part 2: A two-metal binding model as a potential mechanism of HIV integrase inhibitors. *Bioorg. Med. Chem.* **2006**, *14*, 8420–8429.

(34) Kawasuji, T.; Fuji, M.; Yoshinaga, T.; Sato, A.; Fujiwara, T.; Kiyama, R. 3-Hydroxy-1,5-dihydro-pyrrol-2-one derivatives as advanced inhibitors of HIV integrase. *Bioorg. Med. Chem.* **2007**, *15*, 5487–5492.

(35) Grobler, J. A.; Stillmock, K.; Hu, B.; Witmer, M.; Felock, P.; Espeseth, A. S.; Wolfe, A.; Egbertson, M.; Bourgeois, M.; Melamed, J.; Wai, J. S.; Young, S.; Vacca, J.; Hazuda, D. J. Diketo acid inhibitor mechanism and HIV-1 integrase: implications for metal binding in the active site of phosphotransferase enzymes. *Proc. Natl. Acad. Sci. U.S.A.* **2002**, *99*, 6661–6666.

(36) Maurin, C.; Bailly, F.; Buisine, E.; Vezin, H.; Mbemba, G.; Mouscadet, J. F.; Cotelle, P. Spectroscopic Studies of Diketoacids-Metal Interactions. A Probing Tool for the Pharmacophoric Intermetallic Distance in the HIV-1 Integrase Active Site. *J. Med. Chem.* **2004**, *47*, 5583–5596.

(37) Sechi, M.; Bacchi, A.; Carcelli, M.; Compari, C.; Duce, E.; Fiscaro, E.; Rogolino, D.; Gates, P.; Derudas, M.; Al-Mawsawi, L. Q.; Neamati, N. From Ligand to Complexes: Inhibition of Human Immunodeficiency Virus Type 1 Integrase by β -Diketo Acid Metal Complexes. *J. Med. Chem.* **2006**, *49*, 4248–4260.

(38) Bacchi, A.; Biemmi, M.; Carcelli, M.; Carta, F.; Compari, C.; Fiscaro, E.; Rogolino, D.; Sechi, M.; Sippel, M.; Sottriffer, C.; Sanchez, T. W.; Neamati, N. From Ligand to Complexes. Part 2. Remarks on Human Immunodeficiency Virus Type 1 Integrase inhibition by β -Diketo Acid Metal Complexes. *J. Med. Chem.* **2008**, *51*, 7253–7264.

(39) Courcot, B.; Firley, D.; Fraisse, B.; Becker, P.; Gillet, J. M.; Pattison, P.; Chernyshov, D.; Sghaier, M.; Zouhiri, F.; Desmaele, D.; d'Angelo, J.; Bonhomme, F.; Geiger, S.; Ghermani, N. E. Crystal and electronic structures of magnesium(II), copper(II), and mixed magnesium(II)-copper(II) complexes of the quinoline half of styrylquinoline-type HIV-1 integrase inhibitors. *J. Phys. Chem. B* **2007**, *111*, 6042–6050.

(40) Drevensek, P.; Košmrlj, J.; Giester, G.; Skauge, T.; Sletten, E.; Sepčić, K.; Turel, I. X-Ray crystallographic, NMR and antimicrobial activity studies of magnesium complexes of fluoroquinolones – racemic

ofloxacin and its S-form, levofloxacin. *J. Inorg. Biochem.* **2006**, *100*, 1755–1763.

(41) Turel, I.; Živec, P.; Pevec, A.; Tempelaar, S.; Psomas, G. Compounds of antibacterial agent Ciprofloxacin and Magnesium – Crystal structures and molecular modeling calculations. *Eur. J. Inorg. Chem.* **2008**, 3718–3727.

(42) Chen, I. J.; Neamati, N.; MacKerell, A. D., Jr. Structure-based inhibitor design targeting HIV-1 integrase. *Curr. Drug Targets: Infect. Disord.* **2002**, *2*, 217–234.

(43) Maurin, C.; Bailly, F.; Cotelle, P. Structure-activity relationship of HIV-1 integrase inhibitor-enzyme-ligand interaction. *Curr. Med. Chem.* **2003**, *10*, 1795–1810.

(44) Sato, M.; Motomura, T.; Aramaki, H.; Matsuda, T.; Yamashita, M.; Ito, Y.; Matsuzaki, Y.; Yamataka, K.; Ikeda, S.; Shinkai, H. Quinolone carboxylic acids as a novel monoketo acid class of Human Immunodeficiency Virus Type1 Integrase inhibitors. *J. Med. Chem.* **2009**, *52*, 4869–4882.

(45) DeJesus, E.; Berger, D.; Markowitz, M.; Cohen, C.; Hawkins, T.; Ruane, P.; Elion, R.; Farthing, C.; Zhong, L.; Chen, A. K.; McColl, D.; Kearney, B. P. Antiviral Activity, Pharmacokinetics, and Dose Response of the HIV-1 Integrase Inhibitor GS-9137 (JTK-303) in Treatment-Naive and Treatment-Experienced Patients. *J. Acquired Immune Defic. Syndr.* **2006**, *43*, 1–5.

(46) Johnson, A. A.; Marchand, C.; Pommier, Y. HIV-1 integrase inhibitors: a decade of research and two drugs in clinical trial. *Curr. Top. Med. Chem.* **2004**, *4*, 671–686.

(47) Maurin, C.; Bailly, F.; Cotelle, P. Improved preparation and structural investigation of 4-aryl-4-oxo-2-hydroxy-2-butenic acids and methyl esters. *Tetrahedron* **2004**, *60*, 6479–6486.

(48) Sechi, M.; Carta, F.; Sannia, L.; Dallochio, R.; Dess, A.; Neamati, N. Design, synthesis, molecular modeling, and anti-HIV-1 integrase activity of a series of photoactivatable diketo acid-containing inhibitors as affinity probes. *Antiviral Res.* **2009**, *81*, 267–276.

(49) Gatehouse, B. M.; O'Connor, M. J. The crystal and molecular structure of racemic [bis(ethylenediamine)acetylpyruvato]cobalt(III) iodide monohydrate. *Acta Crystallogr.* **1976**, *B32*, 3145–3148.

(50) Kawai, H.; Kitano, Y.; Mutoh, M.; Hata, G. Synthesis, structure and antitumor activity of a new water-soluble platinum complex, (1R, 2R-cyclohexanediamine-N,N') [2-hydroxy-4-oxo-2-pentenoato(2-)-O2]-platinum(II). *Chem. Pharm. Bull.* **1993**, *41*, 357–361.

(51) Barreca, M. L.; Iraci, N.; De Luca, L.; Chimirri, A. Induced-Fit docking approach provides insight into the binding mode and mechanism of action of HIV-1 Integrase inhibitors. *ChemMedChem* **2009**, *4*, 1446–1456.

(52) Liao, C.; Nicklaus, M. C. Tautomerism and Magnesium chelation of HIV-1 Integrase inhibitors: a theoretical study. *ChemMedChem* **2010**, *5*, 1053–1066.

(53) Cremer, D.; Pople, J. A. General definition of ring puckering coordinates. *J. Am. Chem. Soc.* **1975**, *97*, 1354.

(54) Al-Mawsawi, L. Q.; Sechi, M.; Neamati, N. Single amino acid substitution in HIV-1 integrase catalytic core causes a dramatic shift in inhibitor selectivity. *FEBS Lett.* **2007**, *581*, 1151–1156.

(55) Marchand, C.; Johnson, A. A.; Karki, R. G.; Pais, G. C. G.; Zhang, X.; Cowansage, K.; Patel, T. A.; Nicklaus, M. C.; Burke, T. R., Jr.; Pommier, Y. Metal-Dependent Inhibition of HIV-1 Integrase by β -Diketo Acids and Resistance of the Soluble Double-Mutant (F185K/C280S). *Mol. Pharmacol.* **2003**, *64*, 600–609.

(56) SAINT: SAX, Area Detector Integration; Siemens Analytical instruments Inc.: Madison, Wisconsin, USA.

(57) SADABS: Area-Detector Absorption Correction; Siemens Industrial Automation, Inc.: Madison, Wisconsin, USA, 1996.

(58) Altomare, A.; Cascarano, G.; Giacovazzo, C.; Guagliardi, A.; Burla, M. C.; Polidori, G.; Camalli, M. SIR92—a program for automatic solution of crystal structures by direct methods. *J. Appl. Crystallogr.* **1994**, *27*, 435.

(59) SHELXL97: Sheldrick, G. M. SHELXL97. Program for structure refinement; University of Göttingen: Göttingen, Germany, 1997.

(60) Allen, F. H.; Kennard, O.; Taylor, R. Systematic analysis of structural data as a research technique in organic chemistry. *Acc. Chem. Res.* **1983**, *16*, 146–153.

(61) Fiscaro, E.; Braibanti, A. Potentiometric titrations in methanol/water medium: Intertitration variabilità. *Talanta* **1988**, *10*, 769.

(62) Gran, G. Determination of the equivalence point in potentiometric titrations. Part II. *Analyst* **1952**, *77*, 661.

(63) Gans, P.; Sabatini, A.; Vacca, A. Investigation of equilibria in solution. Determination of equilibrium constants with the HYPERQUAD suite of programs. *Talanta* **1996**, *43*, 1739.